MAUSAM, **67**, 4 (October 2016), 767-788

551.553.21 : 551.501.8 (540)

Spatial rainfall patterns associated with Indian northeast monsoon derived from high resolution rainfall estimates of Chennai DWR

B. AMUDHA, Y. E. A. RAJ, R. ASOKAN and S. B. THAMPI

India Meteorological Department, Chennai – 600 006, India

(*Received 3 August 2015, Accepted 21 September 2015*)

e mail : amudha2308@gmail.com

सार – अक्तूबर-नवम्बर-दिसम्बर (OND) की अवधि में भारतीय उत्तरपूर्वी मॉनसून (NEM) ऋतु से प्रायद्वीपीय भारत के दक्षिण पूर्वी भागों को लाभ पहुँचता है। इस अध्ययन में, जो भारतीय क्षेत्र में इस प्रकार की पहली घटना है, भूमि और समुद्र दोनों में फैले 100 कि. मी. के घेरे के गोलाकार क्षेत्र में 12 वर्षों की अवधि (2002-13) के लिए चेन्नै डॉप्लर मौसम रेडार (DWR) द्वारा उत्पन्न किए गए अति उच्च विभेदन (333 m × 333 m) रेडार आकलित वर्षा (RERF) के आँकड़ों का उपयोग करते हुए NEM वर्षा (RF) के कुछ नए और प्रमुख लक्षणों को प्राप्त किया गया है। प्रतिदिन 2.8 लाख से अधिक ग्रिड बिंदु आँकड़े संसाधित किए गए। 34 अंदरूनी स्टेशनों के वर्षा-मापी मापित वर्षा (RGRF) आँकड़ों का भी उपयोग किया गया। अक्तूबर, नवम्बर और दिसम्बर के लिए RERF के मासिकवार स्थानिक वितरणों और पूरी ऋतु के लिए OND तैयार किए गए। वास्तविक विश्लेषण के माध्यम से यह पता चला है कि RERF तट के निकट भारी होते है और स्थल में बताए गए देशांतर के लिए उत्तरी अंक्षाशों की अपेक्षा दक्षिणी अक्षांश 10-15% अधिक RF प्राप्त करता है। बंगाल की खाड़ी (BoB) में पूर्व की ओर RF में धीरे-धीरे कमी होती है जबकि पूर्व की ओर स्थल में इसमें तेजी से और लगभग रेखीय कमी होती है। कुल मिलाकर RGRF के ऐतिहासिक विश्लेषण से प्राप्त किए गए NEM के जलवायविक विशेषताओं को RERF आँकड़ों के आधार पर किए गए विश्लेषण द्वारा अच्छी तरह से दायरे में लिया गया है। मासिक और ऋतुनिष्ठ RF के कुछेक नए लक्षणों का भी पता लगाया गया है। 34 स्टेशनों के लिए OND के 12 वर्षों के आंकड़ा सेट के लिए RERF और RGRF के मानों के औसत मात्र 2.4 मि. मी. की भिन्नता की ओर झुकते हुए क्रमश: 629.8 मि. मी. और 627.4 मि. मी. रहे किंतु इसमें 69.2 मि. मी. की वास्तविक माध्य पूर्ण त्रुटि रही। अक्तूबर के पूर्व NEM के दिनों में RERF का कुल ऋतुनिष्ठ OND का 10% योगदान रहा। चक्रवाती विक्षोभों (CD के दिनों) के दिनों में अध्ययन वाले क्षेत्र में RERF भूमि की अपेक्षा BoB के बाहरी समुद्री क्षेत्रों में लगभग दुगुना रहा है। यह देखा गया है कि RERF, NEM के वापसी के प्रारंभ होने के दौरान DWR के 100 कि. मी. के घेरे में समुद्री क्षेत्रों (68 से. मी.) की अपेक्षा तट के निकट के क्षेत्रों (75 से. मी.) में अधिक रहा है। स्थल में अधिकतम रूप से पश्चिम की ओर 25-30 कि. मी. और समुद्र में पूर्व की ओर लगभग 30-40 कि. मी. के उच्च RF क्षेत्रों को बताया गया है। RGRF आँकड़ों से पता लगाए गए NEM अर्थात शुष्क, कमजोर, सामान्य, सक्रिय और प्रबलता के विभिन्न चरणों के दौरान RERF के स्थानिक वितरणों को तैयार कर विवेचनात्मक रूप से विश्लेषण कर परिणामों को बताया गया है। CD के दिनों को छोड़ कर प्रबल, सक्रिय और प्रबल (AV) NEM के दिनों में, तट के निकट पश्चिम में अधिकतम 5-10 कि. मी. में स्थित 5-6 से. मी. का अपेक्षाकृत उच्च दैनिक RERF का एक क्षेत्र और चेन्नै DWR के SW क्षेत्र में देखा गया। दिसम्बर में NEM की वापसी के दिनों में स्थल क्षेत्रों की तुलना में पूर्वी क्षेत्र के समुद्री क्षेत्रों में उच्चतम RF प्राप्त हुए जो NEM के वापसी पैटर्न के अनुकूल रहे। RERF में त्रुटियों के योगदान में उपकरणीय परिसीमाओं और रेडारों के कौशलों पर विचार विमर्श किया गया।

ABSTRACT. The Indian northeast monsoon (NEM) season benefits the southeastern parts of peninsular India during the period October-November-December (OND). In this study, which is a first of this type for the Indian region, certain new and salient features of the NEM rainfall (RF) have been derived utilising the very high resolution (333 m × 333 m) radar estimated rainfall (RERF) data generated by the Doppler Weather Radar (DWR) at Chennai for the 12 year period (2002-13), over a circular area of 100 km radius spreading over both land and ocean. More than 2.8 lakhs of grid point data per day have been processed. Rain gauge measured rainfall (RGRF) data of 34 inland stations has also been used. Monthwise spatial distributions of RERF for October, November and December and for the entire season OND have been generated. It is shown through rigorous analysis that RERF is heavier closer to the coast and for a given longitude over land, southern latitudes receive 10-15% more RF than the northern latitudes. Decrease of RF eastwards into Bay of Bengal (BoB) is gradual whereas westwards over inland it is sharp and almost linear. By and large, the climatological features of NEM derived from historical analysis of RGRF data are well-captured by the analysis based on RERF data. A few new features of monthly and seasonal RF have also been identified. For the 34 stations, 12 year

data set for OND, the mean RERF and RGRF values are 629.8 mm and 627.4 mm respectively yielding a difference of just 2.4 mm but with a substantial mean absolute deviation of 69.2 mm. RERF during pre-NEM days of Oct contributed to 10% of the seasonal OND total. RERF in the area of study, during days of cyclonic disturbances (CD days) is nearly twice over outer oceanic areas of BoB than over land. It has been shown that during the onset to withdrawal period of NEM, RERF is heavier over areas close to the coast (75 cm) than oceanic areas (68 cm) within the 100 km radius of the DWR. High RF zones approximately extending 25-30 km westwards into land and around 30-40 km eastwards over the ocean have been delineated. Spatial distributions of RERF during the various phases of NEM, *viz*., dry, weak, normal, active and vigorous as identified from the RGRF data have been generated, critically analysed and results drawn. In the case of vigorous, active and vigorous (AV) NEM days excluding CD days, a relatively high daily RERF patch of 5-6 cm located approximately 5-10 km west of the coast inland and in the SW sector of Chennai DWR has been identified. During post-NEM withdrawal days of December, oceanic areas of eastern sector are shown to receive highest RF compared to land areas, a feature consistent with the withdrawal pattern of NEM. The instrumental limitations and artifacts of radars contributing to errors in RERF have been discussed.

Key words – Indian northeast monsoon, Doppler weather radar, Chennai, Rainfall, Reflectivity, Surface rainfall intensity, Precipitation accumulation, Z-R relation, Marshall-Palmer relation, Cyclonic disturbances, Isodop effect.

1. Introduction

The Indian North East Monsoon (NEM) is a smaller spatial scale monsoon confined to parts of South Peninsular India (SPI) and sets in after the withdrawal of South West Monsoon (SWM) from most parts of India. The duration of NEM is taken as three months, October (Oct), November (Nov) and December (Dec) (OND) though NEM rains generally commence only in the second half of Oct and in one-third of the years, spill over to January (Jan) of the next calendar year. Various characteristic features of the NEM have been widely researched and the list is exhaustive, few being IMD (1973); Raj (1992, 1998a&b, 2003 and 2012); Pankajkumar (2006) and Geetha (2011). The normal date of onset (DO) and date of withdrawal (DW) of NEM over Coastal Tamil Nadu (CTN) re-determined based on rainfall (RF) data of the period 1901-2000 are 20 Oct and 30 Dec respectively (Geetha and Raj, 2015). Tamil Nadu (TN) is the major beneficiary of NEM receiving 48% (438 mm) of its annual RF of 914 mm during OND [IMD (2010) & Raj (*loc.cit*.)].

Technological breakthroughs in remote sensing and their applications in weather forecasting marked the beginning of a new chapter in exploratory research in atmospheric sciences. Weather satellites which were launched first in the early 1960s provided cloud imageries and enabled observing weather over the earth from the skies. The present day weather satellites orbiting the earth are highly sophisticated and deliver several weather products and by-products. The weather radar is another remote sensing marvel which can be operated in all-weather conditions to map the profile of the atmosphere over the neighbourhood where it is installed. The technological capabilities of weather radars have increased over the years and those of the present generation provide voluminous data of wide variety and reach. Research based on such radar generated weather products has increased considerably and radar meteorology itself has emerged as a separate sub-area of atmospheric sciences.

India Meteorological Department (IMD) is one of the few National Meteorological Services which embraced radar technology for meteorological purposes as early as in the late 1940s with the acquisition of surplus radar equipments after the Second World War. Since then, various types of radars have been inducted and operationally utilised for tracking weather events. Using the 5-year data of the period 1964-69 recorded by a Decca Type-41, 3-cm wavelength radar installed in 1959, an early study on the radar climatology of Madras airport and its neighbourhood was attempted by Lakshmanaswamy and Sundaresa Rao (1974). Studies using data from analogue radars, for cities like New Delhi - Kulshrestha and Jain (1967), Kolkata (then, Calcutta) - De and Rakshit (1961) and Mumbai (then, Bombay) - Mukherjee *et al*. (1977) have been conducted.

A conventional S-band Mitsubishi make RC-32E type analogue radar was installed in the year 1972 in Madras (now, Chennai) Port Trust premises. Utilising the data generated by this radar, Raghavan and Varadarajan (1981) analysed the radar estimated rainfall (RERF) characteristics of tropical cyclones of Bay of Bengal (BoB). Raghavan and Sivaramakrishnan (1982) and Raghavan *et al*. (1987) used digitised products of the analogue radar of Madras to derive the relationship between radar reflectivity and RF rate for NEM and SWM respectively. Raghavan (2003) in his comprehensive treatise on radar meteorology has indicated that in the early days of induction of radars in IMD for weather monitoring, restrictions existed in the observational schedules for operating the analogue radars on a full-time basis mainly imposed by technological constraints. The data available for research was only of those active periods of observation which the researchers had to

reconcile with at that time. Under IMD's modernisation programme and upgradation of hardware, the old S-band radar of Madras was replaced with a new digital Doppler Weather Radar (DWR) operating in S-band (2875 MHz) with a wavelength λ = 0.10428 m [Bhatnagar *et al*. (2003)]. This DWR which is sited atop the Port Trust building, Chennai at an altitude of 53 metres above m.s.l. was put into operational use w.e.f. 20 February, 2002.

Chennai city with an area of 178 sq.km. lies within 80.20 - 80.32° E and 12.15 - 13.15° N stretching up to a distance of 25.6 km North-South (N-S) along the BoB coast. Basic meteorological observations commenced as early as in 1793 in Nungambakkam (13.06° N / 80.25° E, NBK) which receives an annual RF of 139 cm with a major contribution of 88 cm from NEM season as per climatological normals of the period 1951-2000 (IMD, *loc.cit*.). Chennai city has a tropical climate with maritime influence, due to its location on the BoB coast. Stations of north CTN experience RF climatology similar to that of Chennai.

The DWRs are capable of mapping the profile of the atmosphere around their locations and providing various weather and hydrological products of instantaneous use to a wide spectrum of users. Very advanced and sophisticated products are available from digital DWRs compared to analogue radars. Technical specifications and salient features of Chennai DWR have been described in Bhatnagar *et al.* (*loc.cit*.) and Rajesh Rao *et al*. (2004). Modern digital DWRs are operated round the clock and throughout the year unless otherwise interrupted by maintenance schedules or unforeseen technical snags. A DWR maps the time evolution of weather events in the neighbourhood of its installation. Chennai DWR is one such radar in continuous operation since its installation generating a large quantum of weather data. Among the several products generated by a DWR, Precipitation Accumulation (PAC) is an important output reliably providing RERF at a very high resolution for a distance of 100km from the radar location. There is tremendous scope of using the data of Chennai DWR especially the PAC data to understand and unravel characteristic features of RF distribution during the NEM season which is associated with maximum RF activity over Chennai and surrounding areas. The voluminous data generated by Chennai DWR have been systematically archived.

The RF characteristics of NEM have already been studied extensively based on rain gauge measured rainfall (RGRF) data which is available since 1871. Several new features of NEM have been brought out in recent studies using satellite based outgoing long wave radiation (OLR) data [Suresh and Raj (2001); Raj *et al*. (2007); Amudha *et al*. 2016(a&b)]. RGRF data and estimates of RF by satellites are of coarser resolution than that obtained with a DWR. Another advantage of a DWR located on the sea coast in comparison with a surface-based conventional rain gauge (RG) is that RF estimates over ocean in the neighbourhood of the DWR location are also available in near-real time basis. There is vast scope for studying NEM RF variability in and around Chennai with the high resolution daily PAC product data of the DWR available since 2002.

With this background on Chennai DWR and its products, the objective of this study is to utilise for the 12 year period 2002-13, the PAC product of Chennai DWR and study the RERF distribution around Chennai during the NEM season. The daily RERF (DRERF) values for the above period have been processed to derive monthly and seasonal RERF figures to identify various climatological features of NEM some of them hitherto unknown. The RERF pattern during the pre-NEM onset days of Oct, that during the duration of NEM from DO to DW, spatial variability during various phases of NEM, *viz*., dry, weak, normal, active and vigorous, influence of the days of cyclonic disturbances (CDs) over BoB, illustration of its variability close to the coast, the mean pattern in Dec after withdrawal of NEM, the instrumental limitations and artifacts contributing to errors in RERF are elaborately discussed in the forthcoming sections and the results derived have been summarised.

2. Radar as a tool for estimation of rainfall

2.1. *Principles of radar-based rainfall estimation*

Radar works by transmitting pulses of radio energy, which are focused by the antenna into a narrow beam. When the beam intercepts a target such as RF, some of its energy is scattered back to the antenna and detected by the radar receiver as echo power. Received echo power, a function of many factors, is converted into an independent characteristic of RF, *viz*., reflectivity factor *Z*, using the famous Probert-Jones Radar Equation (1962). The parameter *Z* is converted to rain rate (*R*), through an empirical *Z*-*R* relationship. For a raindrop of diameter *D*, the echo power is proportional to D^6 whereas the water content is proportional to D^3. *Z* is converted to *R* as both are functions of *D*. Any type of RF contains millions of drops, tiny droplets to large ones, with highly varying Size versus Number-distribution. Hence, the *Z*-*R* relation $Z = AR^b$ according to Marshall-Palmer (1948) is a varying function of drop-size-distribution (DSD) where *Z* is in mm^6/m^3, *R* in mm/hr, *A* & *b* are numerical constants attaining values depending on the DSD. When the DSD details are unavailable and the type of precipitation is predominantly stratiform, *A* = 200 and *b* = 1.6 are the most commonly used values.

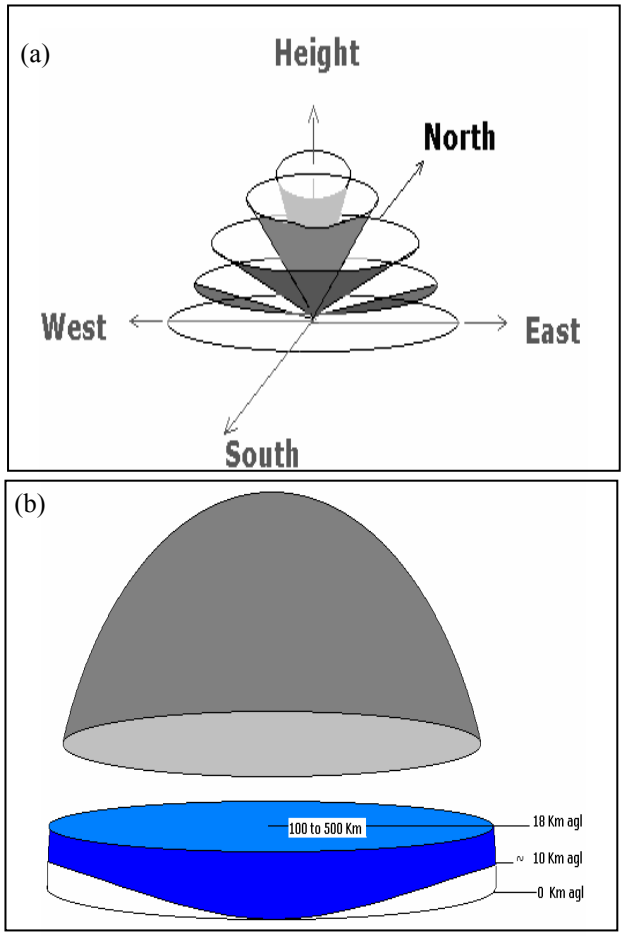

Figs. 1(a&b). (a) Stepping up of elevation angles of the radar antenna in volume scan strategy and (b) the quasi-cylindrical shape of the volume of data scanned

TABLE 1

Dates of onset / withdrawal and seasonal rainfall of Tamil Nadu during NEM, 2002-03 to 2013-14

Year	Date & month of		Rainfall (mm)	
	onset	withdrawal	Actual	PDN
2002-03	09 Oct	12 Dec	396	-8
2003-04	19 Oct	08 Dec	435	-7
2004-05	18 Oct	16 Dec	435	1
2005-06	11 Oct	21 Dec	772	79
2006-07	17 Oct	14 Dec	497	15
2007-08	19 Oct	07 Jan	520	20
2008-09	12 Oct	21 Dec	564	31
2009-10	29 Oct	26 Dec	482	12
2010-11	29 Oct	06 Jan	607	41
2011-12	24 Oct	10 Jan	537	22
2012-13	18 Oct	11 Jan	368	-16
2013-14	21 Oct	18 Jan	293	-33
12 years (2002-13) mean	19 Oct	29 Dec	492 mm	13
Long term (1951-2000) normal	20 Oct	30 Dec	438 mm	

Oct : October, Nov : November, Dec : December, Jan : January
NEM : northeast monsoon PDN : Percentage departure from normal
Rainfall is for the duration 1 Oct-31 Dec.
Range in yearly normals (2002-13) used for computation of PDN : 432 - 469 mm

2.2. *Radar data acquisition sequence or scan strategy*

Dual degree of freedom (both vertical and horizontal) for the antenna facilitates the radar beam to be swept around in different elevations angles. Present scan strategy of Chennai DWR consists of ten complete azimuth sweeps (on completion of each sweep the elevation angle is stepped up by a predetermined increment) lifting the elevation angle [Fig. 1(a)] from near horizontal to about 21°. Data thus acquired forms a quasi-cylindrical volume [Fig. 1(b)] of Z values, which are in turn converted into values of R using the Z-R relation. Due to the curvature of the earth, while looking away from the radar, even for the lowest sweep, access is denied below a certain height for rain events far away. Also as the angle of the highest elevation sweep is limited to around 21°, access to an overhead conical region is forbidden and so the data volume is quasi-cylindrical in shape. The data is acquired in polar (r, Θ, Φ) form. direction of the range or distance from the radar, the spatial resolution of data is set generally to values between 0.5 and 2 km. While sweeping in azimuth, the angular coverage is a function of radar beam-width (1° for the Chennai DWR). Thus, the spatial resolution of the base data is say, ~1 km × 1°.

In the post-processing stage, the base data in polar form is mapped to a Cartesian Space. From the 3D volume data, R pertaining to a surface layer (SL) of equal height from underlying surface is extracted and used as a derived product called Surface Rain Intensity (SRI). For SL height of 1 km, lowest and highest elevation angles 0.5° and 21° respectively, the farthest visible range is ~100 km and the nearest visible range is ~5 km as stated in Amudha *et al*. (2014). It takes about 10 minutes to acquire one full set of volume data. Thus, for a whole day there can be 144 SRI products. Time integration of these 144 sets of SRI data provides a new product called PAC. In this study, PAC for the 24 hour period from 0300 UTC of previous day to 0300 UTC of the current day is used as the RERF data.

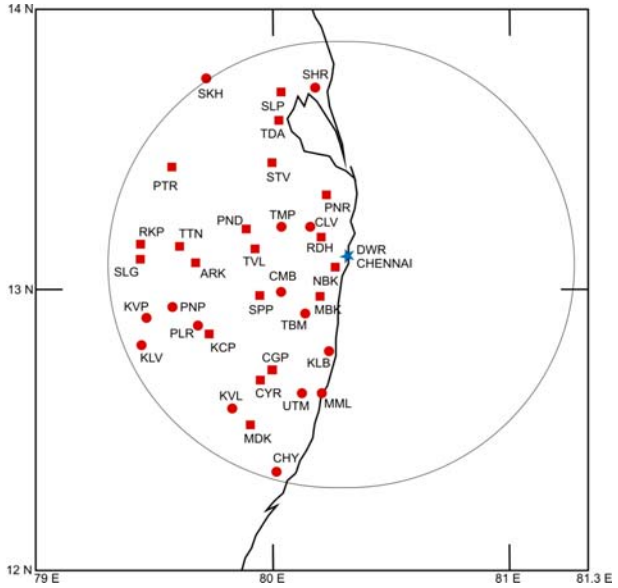

Fig. 2. Spatial distribution of the 34 RG stations over land within 100 km radius of DWR, Chennai ('■' indicates stations with long term normals)

2.3. *Validation of RERF estimates*

For a reasonable judgment of the errors involved in the RERF, the standard used is the conventional RG. Conceptual differences however exist in the methods of RF measurement by a RG installed in the ground level and the RERF pertaining to 1 km SL derived from Z. Rinehart (1991) has observed that there are numerous limitations in these estimates due to various physical and instrumental factors. In spite of such inherent aspects, the RG is used as a standard reference to quantify radar / satellite derived RF uncertainty (Raghavan, 2003). In general, RG and radar are complementary to each other with the advantages outweighing the limitations of both techniques.

Validation studies using RGRF data of stations in the 100 km vicinity of DWR Chennai were first undertaken by Suresh *et al.* (2005), considering the variations in DSD of RF during the period 1 March to 31 Dec, 2003. A best fit regression equation was derived and new values of A = 267 and b = 1.345 in the Z-R relationship $Z = AR^b$ were used in the computational software for deriving the RERF data. These values are used in DWR, Chennai for operational generation and archival of base and derived products. Another validation study for a longer period 2006-10 for the pre-monsoon (Mar-May) and NEM seasons was undertaken by Amudha *et al.* (2014) using RGRF data of 16 stations in the 100 km range of the DWR for the days when both RERF and RGRF were available for the pre-monsoon and NEM days. The value of correlation coefficient (CC) was 0.80 between RERF and RGRF, with a mean absolute deviation (MAD) of 6.8 mm indicating underestimation by the radar during the period of study. Chennai DWR due to its coastal location is able to provide crucial and reliable RF estimates on a continuous basis over the adjoining BoB up to 100 km where obviously no conventional RG observations are available. Over land too, the DWR is superior in capturing the finer details of granularity of spatial variations in RF.

TABLE 2

CDs over BoB contributing to various phases of NEM during 2002-13

No.	Year	CD	Duration	NEM activity	
				Dates	Type
1	2002	SCS	10-12 Nov	10 11	A N
2.	2005	DD	26-29 Oct	26 27,28	A V
3.		D	20-22 Nov	21	N
4.		CS Bazz	28 Nov - 2 Dec	2	N
5.		CS Fanoos	6-10 Dec	10	N
6.		DD	15-21 Dec	17	N
7.	2006	CS Ogni	29-30 Oct	29 30	V A
8.	2007	D	27-28 Oct	28 29	A V
9.	2008	CS Khai-Muk	13-16 Nov	16	A
10.		CS Nisha	25-27 Nov	26	V
11.	2010	SCS Jal	4-8 Nov	7 8	N V
12.		DD	7-8 Dec	7	V
13.	2011	VSCS Thane	25-31 Dec	30	V
14.	2012	CS Nilam	28 Oct - 1 Nov	30	N
15.	2013	D	13-16 Nov	16 18	N A
16.		VSCS Lehar	23-28 Nov	23-25	N
17.		VSCS Madi	6-13 Dec	12	N
			Total days	26	

CD : Cyclonic Disturbances, BoB : Bay of Bengal.

D : Depression, DD : Deep Depression, CS : Cyclonic Storm,

SCS : Severe CS, VSCS : Very SCS.

Phases of NEM : N : Normal, A : Active, V : Vigorous

N, A, V defined for the land area within the 100 km radius of Chennai DWR

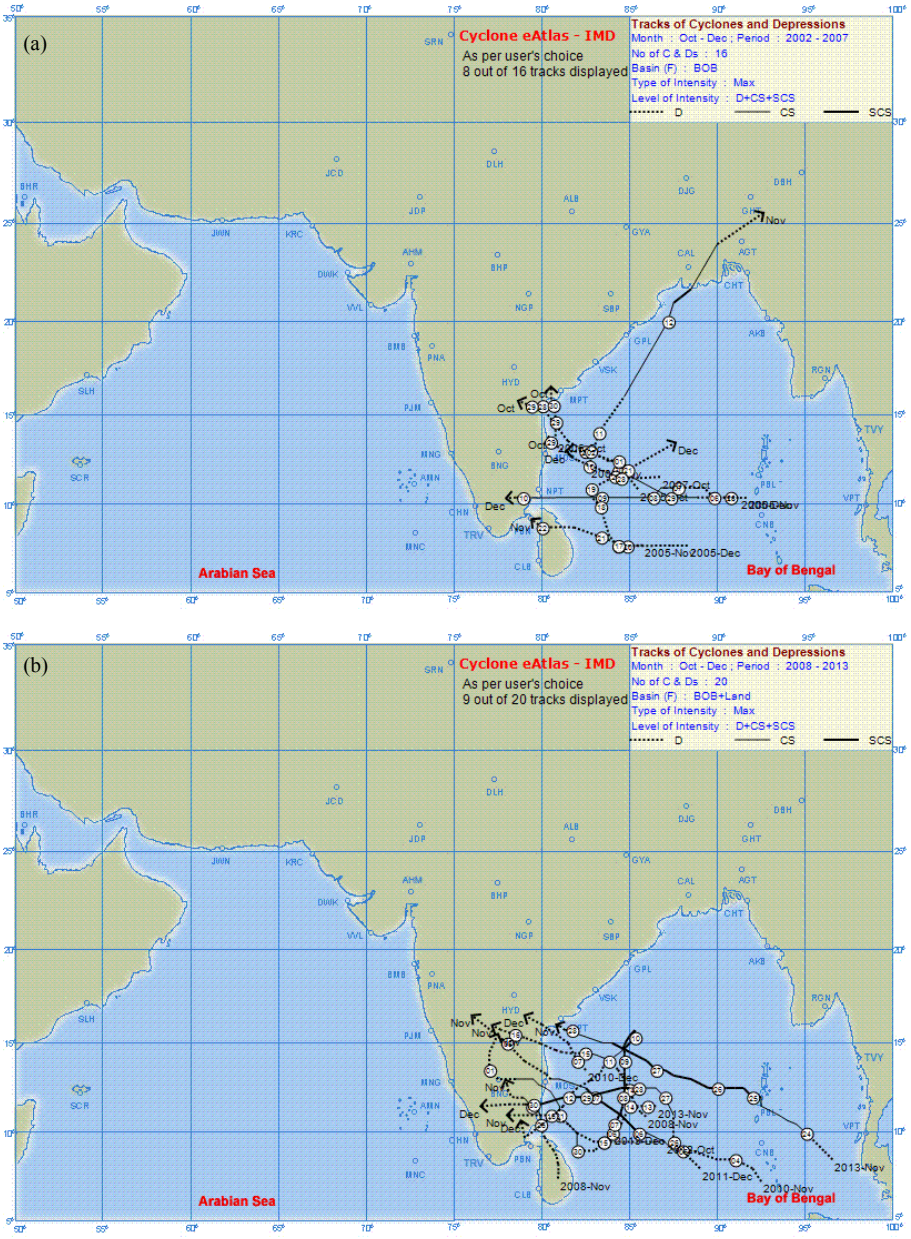

Figs. 3(a&b). Tracks of 17 CDs which originated over BoB / Sri Lanka and contributed to higher RF activity near Chennai DWR during the NEM season, 2002-13 (a) 2002-07 (CDs : 8) and (b) 2008-13 (CDs : 9)

3. Data used

In the present study, the following data have been used.

3.1. The DO and DW of NEM as determined by Geetha and Raj (2015) for the period 2002-13 (Table 1).

3.2. Daily RF (DRF) data from 1 October to 31 December of the 12 year period of 2002-13, for 34 stations located in Tamil Nadu (TN) and Andhra Pradesh (AP) within the 100 km range of Chennai DWR. The spatial distribution of these stations and the geographical location of Chennai DWR are depicted in Fig. 2.

3.3. The long term DRF normals for the period 1951-2000, for 20 stations distinctly identified out of the 34 stations indicated in Fig. 2, were obtained from National Data Centre, Pune (IMD, 2010).

TABLE 3

Configuration and processing details of the PAC product generated by Chennai DWR

Feature	Details
Displayed parameter	Rain accumulation from PAC product of DWR for 24 hours ending at 0830 hrs IST (0300 UTC)
Data domain :	
(a) Centre	DWR Chennai (Long. 80.2899° E Lat.13.0838° N)
(b) Areal extent	Region bounded by a circle of radius 100 km with its centre at DWR Chennai
(c) Surface layer	A curvilinear surface 1 km above the ground right below. As the earth's surface undulates, the surface layer too undulates keeping 1 km height always
(d) Spatial resolution	200 km represented by 600 pixels in both East-West and North-South directions (333 m × 333 m)
Number of data points per PAC	$\pi \times (100000\ m)^2$ / (333 m × 333 m) = ~ 283310 (Nearly half lie over the oceanic area of BoB)
Number of PAC products processed	1 PAC/day × 92 OND days/year × 12 years = 1104
Total data points processed	1104 × 2.83 lakhs = ~ 312 million

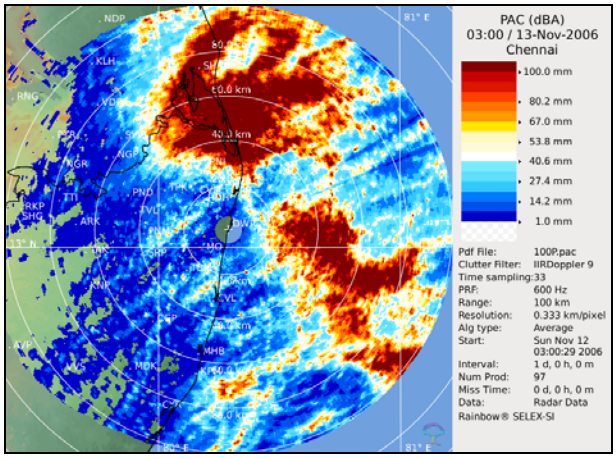

Fig. 4. A sample image of the 24 hours PAC product (in dBA) for the period ending at 0300 UTC of 13 November, 2006 generated by DWR Chennai

3.4. RF expressed as percentage departures from normal (PDN) for the NEM season (1 Oct - 31 Dec) for TN (Table 1) obtained from Regional Meteorological Centre (RMC), Chennai. RF of TN is generally taken as an index of NEM activity over CTN and hence for the region of our study.

3.5. Details of CDs that occurred during 2002-13 over BoB / North Indian Ocean (NIO) (IMD, 2011, Cyclone e-Atlas) presented in Figs. 3(a&b) and Table 2.

3.6. Grid point data of the PAC product generated daily by Chennai DWR, for Oct, Nov and Dec for the 12 year period 2002-13 at a spatial resolution of 0.333 km/pixel in both directions. Fig. 4 is a sample of the daily PAC image generated for the 24 hrs period ending at 0300 UTC (0830 hrs IST) of 13 November, 2006.

4. PAC configuration, data artifacts and quality control measures opted for this study

Details of the PAC configuration and artifacts in the data are explained in this section.

4.1. *PAC specifications*

The PAC data is generated with configuration settings as given in Table 3.

4.2. *Data contaminants and quality control*

As the RERF is prone to many forms of contamination and misrepresentation caused by echoes of non-precipitation origin and temporal variations in the radio propagation characteristics of the atmosphere, many grid points of the daily PAC product may contain spurious values of high or moderate RF values (Rajesh Rao *et al.*, *loc.cit.*). Spurious echoes which occasionally contributed to very high RF rates were eliminated from the text data files by following a procedure of manually flagging such spurious values and removing them from the text data. The final quality controlled daily output files containing RF (in mm), almost bereft of such spurious values were used for further analysis.

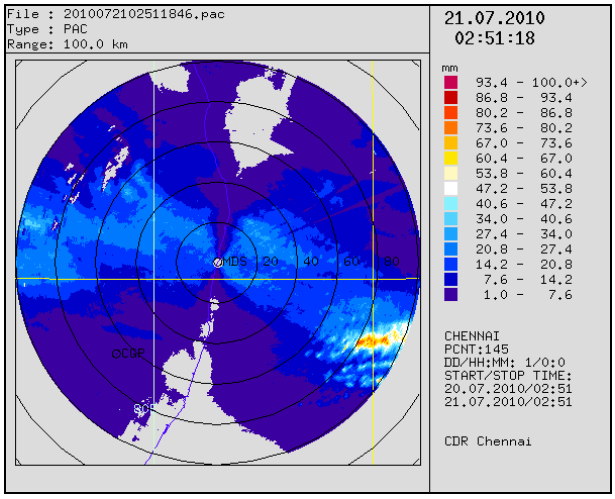

Fig. 5. Illustration of zero isodop effect along NNE-SSW direction with Chennai DWR as centre leading to underestimation of rainfall in the daily PAC product

4.3. *Data artifacts*

4.3.1. *Beam blockage and mirror effect*

A few wedge-shaped narrow sectors of distinctly different RF estimates visible in the PAC image on fairly widespread rainy days are due to blocking of the radar beam by solid objects like tall semi-permanent cranes of Chennai Port Trust (NE quadrant), TV tower (South of South West octant), Chimneys of thermal power plants [North West (NW) quadrant] and a few mobile communication towers. These distinct RF values are mostly under-estimations and at times over-estimations due to mirror effect wherein echoes of rain drops from diametrically opposite directions reach the receiver due to reflection of the transmitted pulse by these solid objects which act as obstructions. Care was taken to avoid or account for these artifacts while performing RERF analysis and drawing inferences from the patterns obtained.

4.3.2. *Zero isodop effect*

To get rid of spurious reflectivity and the resulting erroneous RERF values contributed by strong non-precipitation echoes mostly from stationary objects, their near-zero Doppler velocity is exploited to identify and eliminate or attenuate them significantly. When such a velocity based clutter filter technique is used for all data points indiscriminately, along with undesired echoes from static clutters, some real value echoes (from those rain drops moving tangential to the radar beam with near zero radial velocity) also would get filtered out or significantly attenuated. On days with preferred large-scale winds in the radar field, echoes in two diametrically opposite sectors orthogonal to the prevailing wind direction would continue to have near zero radial velocity and hence get attenuated repeatedly. At the end of the day when all such RF samples are integrated to build a PAC product, such an artifact due to zero isodop effect (Nan and Ming, 2010) leading to subdued RF would emerge. An illustration of zero isodop effect on 21st July, 2010 when WNW wind prevailed causing suppression of RERF in NNE-SSW sectors is provided in Fig. 5.

The same artifact could also build-up in a monthly or seasonal average PAC product, if a preferred wind direction existed for the month and the season. It is well known that during the active NEM season, the preferred wind direction over Chennai region is from northeast (NE). As DWR Chennai has been using the Doppler clutter filter all along, subdued RF values in the NW and SE sectors could be expected in daily, monthly or even seasonal average PAC images. This effect wherever manifested during data analysis is identified and mentioned in the relevant sections.

5. Methodology of computations and analysis

The text data of the daily PAC product for the period of study were processed using FORTRAN and converted to Grid Analysis and Display System (GrADS) compatible format for graphical analysis, visualisation and pattern recognition. Using the DRERF extracted from the PAC product, the mean RF distributions for the months of Oct, Nov and Dec and for the NEM (OND) season of the period 2002-13, over the grid points in the area of consideration were computed and are presented in Figs. 6(a-c) and Fig. 7(a). A large number of such maps on RERF were generated for various types of NEM activity also. The features observed are discussed in the following sub-sections.

5.1. *Monthly distribution of mean RERF*

Oct : In Fig. 6(a) the land area between 79.4-79.8° E shows mean RERF of 20-30 cm except for patches in the NW sector with 10-20 cm. Areas closer to the coast, receive higher RF of 30-40 cm. Over the oceanic longitudes of 80.3 - 81.2° E, the NE sector 13-14° N has significant areas of RF in the range of 40-50 cm while the rest of the areas are in 30-40 cm range. In the southeast (SE) sector of BoB, RERF is 30-40 cm with few scattered patches of 20-30cm. Underestimation of RERF is evident in certain sectors of Fig. 6(a) due to beam blockage as mentioned in Section 4.3.1.

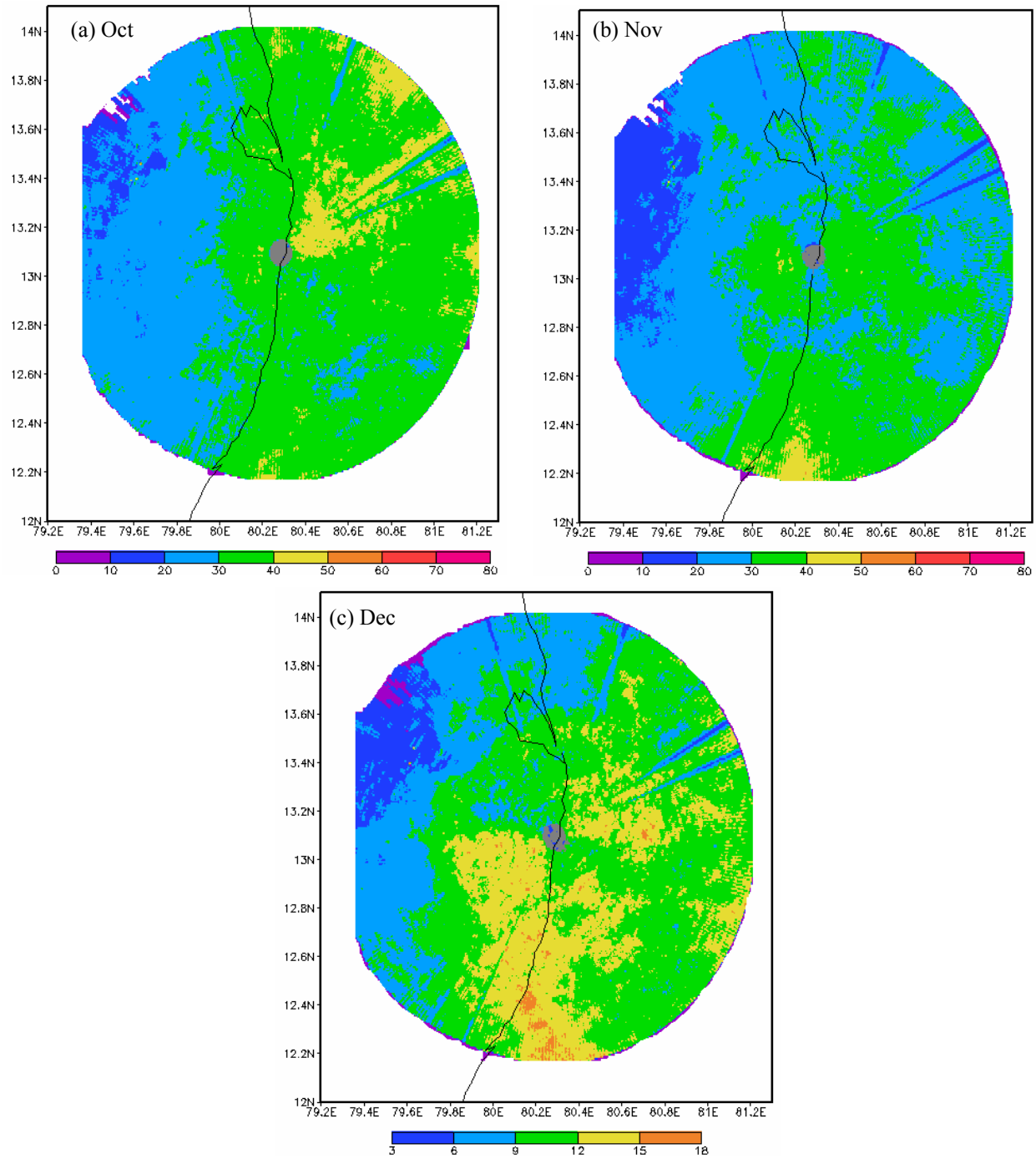

Figs. 6(a-c). Distribution of monthly mean RERF (cm) for (a) Oct, (b) Nov and (c) Dec, 2002-13

Nov : The rainiest month over CTN is Nov and is representative of NEM season. The RERF distribution [Fig. 6(b)] reveals that over land the southern and SW sectors of Chennai DWR formed by 79.9-80.1° E and 12.2-13.2° N receive RF of 30-40 cm. Major portions of the land area westwards register RF of 20-30 cm. RF decreases to 10-20 cm from east-west (E-W) of the DWR along 79.4 - 79.6° E and 12.8 - 13.8° N. Over ocean, a tiny portion of the southern sector 79.8 - 80.3° E up to 12.3° N along the BoB coast has a distinct patch of 40-50 cm RF while a vast area of BoB has RF of 30-40 cm in the SE / NE sectors with scattered zones of 20-30 cm RF in the eastern sector of the Chennai DWR.

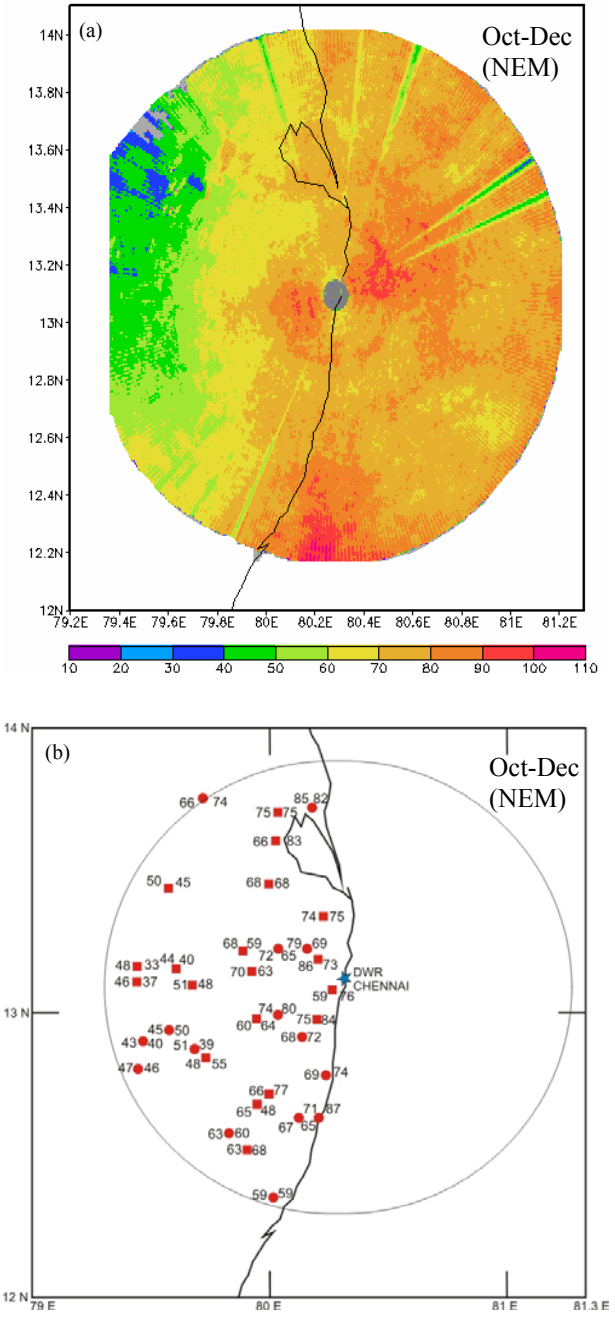

Figs. 7(a&b). Distribution of (a) mean RERF (cm) for OND, 2002-13 (b) RERF (*x*) and RGRF (*y*), at the grid points of 34 stations plotted as per legends '*x* ■ *y*' and '*x* ● *y*' (Refer Fig. 2 for station ID)

The conical beams of underestimation of RF in the ocean are due to beam blockage as explained in Section 4.3.1. The clear-cut diagonal patch of low RF (20-30 cm) along NW-SE centered at the DWR location is due to the zero isodop effect which is described in Section 4.3.2.

Dec : The decrease in RERF marked by the withdrawal phase of NEM during Dec is evident from Fig. 6(c). Over land, in the SW sector of the DWR, there is gradual decrease of RF from 12-15 cm close to the coast to 3-6 cm westwards. RERF close to the coast in the NW sector (9-12 cm) is less than that of the SW sector (12-15 cm). In most parts of the oceanic area, RERF > 9 cm is seen with zones of 12-15 cm and smaller patches of 15-18cm. The conical beams of under-estimation of RF as described earlier are seen in Dec also.

It is worthwhile to note that the isodop effect is observed for the distribution of Nov and Dec but absent for Oct where the first half of the month is characterised by prevalence of SW winds in the lower levels and NE winds set in much later.

5.2. *Mean seasonal distribution of RERF*

On a seasonal scale, RERF for OND for the entire area of consideration is depicted in Fig. 7(a). Since this distribution is of very high resolution (333 m per grid point), it is possible to identify new features of NEM RF hitherto unknown. Some of the inferences drawn from Fig. 7(a) are as under:

5.2.1. *Over land*

(*i*) The RERF is heavier over/closer to the coast.

(*ii*) Along a given latitude, the RERF by and large decreases from E-W over land.

(*iii*) Along a given longitude, the latitudes south of DWR receive 10-15% more RF than the northern latitudes.

(*iv*) RERF zones of 80-90 cm and smaller patches of 90-100 cm are observed in the SW sector of DWR location.

(*v*) The RERF decreases inland to 70-80 cm, then to 60-70 cm at 79.8° E and it reaches 50-60 cm roughly west of 79.7° E.

5.2.2. *Over the ocean*

(*i*) The heaviest RERF zones of 80-90 cm and within that patches of 90-100 cm are seen in the NE sector of DWR location. Another heavy RERF zone is seen over the extreme south just east of the coastal belt.

(*ii*) East of 80.8° E the RERF over the ocean is lower than that adjacent to the coast. But the decrease further east is gradual and not uniform.

(*iii*) Lowest amount of RERF is 60-70 cm in small patches.

Features of the mean OND (NEM) RERF distribution over land derived in this study compare very well with that of RGRF distribution for OND based on long term climatology (IMD, 1973; Raj, 2012). The OND seasonal RERF is generally heavier over the coast and decreases westwards inland and this feature has been brought out in the mean RERF distribution very well.

Since the focus of this study is to analyse the RERF distribution on monthly and seasonal scales, a comparison between the climatologies based on RERF and RGRF is desirable. The mean RERF values for OND at the geo-coordinates of each of the 34 stations were extracted from the text file used to generate Fig. 7(a). Using the monthly cumulative RGRF data, the seasonal OND means for each of the 34 stations illustrated in Fig. 2 were also computed depending upon the number of years of RGRF data available during the 12 year (2002-13) period. The mean values of RERF and RGRF thus generated for the stations are depicted in Fig. 7(b) and a comparative analysis between the two types of averages led to the following inferences:

(*i*) The mean RGRF computed varies between 327.2 mm (RKP : R. K. Pet) and 865.1 mm (MML : Mamallapuram). The mean RERF at the 34 stations varies between 426.0 mm (KVP: Kaveripakkam, just south of R. K. Pet) and 857.0 mm (RDH: Red Hills).

(*ii*) The mean RERF is 629.8 mm and the mean RGRF is 627.4 mm (averaged over the 34 stations) yielding a difference of just 2.4 mm or 0.4% of mean RGRF.

(*iii*) The difference RERF-RGRF is positive at 20 locations and negative at 14 locations. The MAD is 69.2 mm which is 11% of the mean RGRF.

(*iv*) The CC between RERF (x) and RGRF (y) is 0.82 and is highly significant.

It is seen that even when we consider seasonal mean, station to station difference between the two types of RF is substantial, as evidenced by the MAD of 69.2 mm though spatial averaging over the region does bring down the difference to a large extent. Needless to say that when we consider monthly and seasonal RF figures year-to-year, the differences between the two types of RF would still be larger. Since it is essential to critically analyse such differences also for the correct usage and interpretation of RERF, a detailed and independent study with a different focus from the present one, has been undertaken and results published separately.

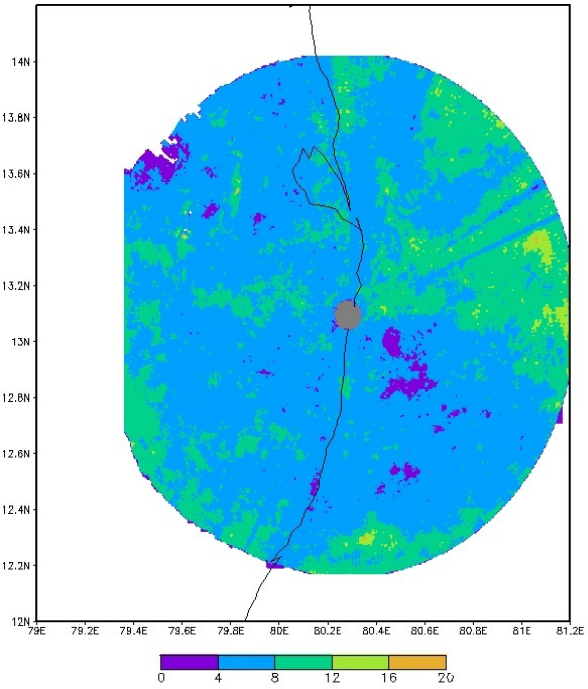

Fig. 8. Distribution of cumulative mean RF (cm) for pre-NEM onset days of Oct, 2002-13

5.3. *Mean RERF pre- and post-NEM onset*

By convention, the NEM seasonal RF total is accounted from 1 Oct to 31 Dec. However, the normal DO of NEM is 20 Oct with a standard deviation of 7-8 days. During the period of analysis, onset of NEM took place in Oct in all the years with 19 Oct as the mean date as shown in Table 1. The RF which is realised from 1 Oct up to the DO of NEM, associated with lower level SW winds not possessing NEM characteristics also gets included in the seasonal total RF. It is preferable to study separately and bring out distinct features of the variation of RERF during the pre-NEM phase in Oct and also the pattern of RF strictly during the duration of NEM, *i.e.*, from DO to DW, named here as post-NEM onset.

5.3.1. *Mean RERF pattern during pre-NEM days of Oct*

To derive the quantum of RF that occurs during the pre-NEM onset phase, the days from 1 Oct to the day just prior to the DO during 2002-13 were identified and RERF was cumulated for each year and averaged over 12 years. There were 214 such days during the study period. This analysis was carried out for every grid point and the resulting spatial distribution of cumulative RF (CRF) is presented in Fig. 8. As seen, over most of the land area, the mean CRF is 4-8 cm with few smaller patches registering 8-12 cm. Over the ocean, the mean

RERF in the NE sector is nearly 8-12 cm with regions of higher RF of 12-16 cm and 16-20 cm in the east-NE sector. In the SE sector around 40 km away from coast and over the ocean, RF is lower at 4-8 cm with a small zone receiving less than 4cm. The high quantum of rain in the NE sector is probably due to the presence of feeble systems over BoB when the surface equatorial trough is on its southward progression during the first half of Oct. It is also worthwhile to note that the belt of relatively high RF over CTN observed during NEM is missing in the distribution of pre-NEM RERF.

5.3.2. *Mean RERF pattern during post-NEM onset (the duration of NEM)*

To derive the average spatial CRF pattern during post-NEM onset (NEM duration), the period from DO to DW (DW was taken as 31 Dec if it was later) only was considered. Overall, 791 days of NEM were included in the analysis. The DRERF cumulated for each year was used to compute the 12 years mean CRF for each grid point. The spatial distribution of mean RERF for the duration of NEM is presented in Fig. 9.

Inferences drawn from an evaluation and comparison between the features of NEM observed in both Fig. 7(a) and Fig. 9 are provided below:

5.3.2.1. *Over land*

(*i*) Features related to seasonal OND total [Fig. 7(a)] RERF described in (*i*), (*ii*) and (*iii*) of Section 5.2 hold good for the CRF during DO-DW also.

(*ii*) Compared to CRF of OND [Fig. 7(a)] over both land and ocean, a reduction in RERF of 10-20 cm is observed in Fig. 9.

(*iii*) Maximum RERF of 80-90 cm is observed just 5-10 km away from the coast in the SW sector of Chennai DWR location.

(*iv*) Zero isodop effect as detailed in Section 4.3.2 is observed in Fig. 9.

5.3.2.2. *Over ocean*

(*i*) NE and SE sectors from the DWR location have higher RERF of 70-80 cm possibly caused by the influence of CDs of the BoB. RERF decreases to 60-70 cm beyond 80.7° E (Fig. 9).

(*ii*) There is a distinct patch of RERF > 90 cm in the NE sector, just a few km away from the coast between 80.3 and 80.5° E.

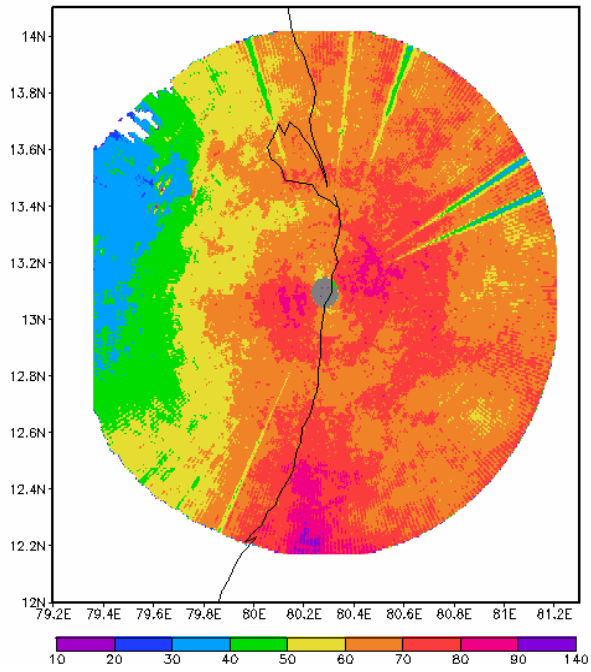

Fig. 9. Distribution of cumulative mean RERF (cm) during DO-DW (Dates of onset and withdrawal), 2002-13

(*iii*) Higher RERF zone of 80-90 cm south of the DWR location extending up to the periphery of the area of consideration and a very small inner patch of RERF > 90 cm are observed.

(*iv*) A conspicuous difference in the RF patterns displayed by Figs. 7(a&b) is that the NE sector over ocean with reference to the DWR location is much less rainy in the latter compared to the former which takes into account all the 92 days of the season. That the NE sector received relatively more RF in the pre-NEM onset days of Oct (Fig. 8) is the obvious reason.

For further detailed analysis, the mean RERF distribution averaged over all the latitudes of the area under consideration for a given longitude was generated and is depicted in Fig. 10(a). The RERF distribution at the latitude 13.1° N of Chennai DWR also has been extracted and presented in Fig. 10(b).

Inferences drawn from Figs. 10(a&b) are as under:

(*i*) The peaking of RERF close to the coast, the sharp near-linear decrease of RF westwards into the land, the constant RERF profile for nearly 40 km eastwards from the coast into the ocean and the slow decrease of RERF further eastwards-these features have been captured and depicted with better clarity in Fig. 10(a).

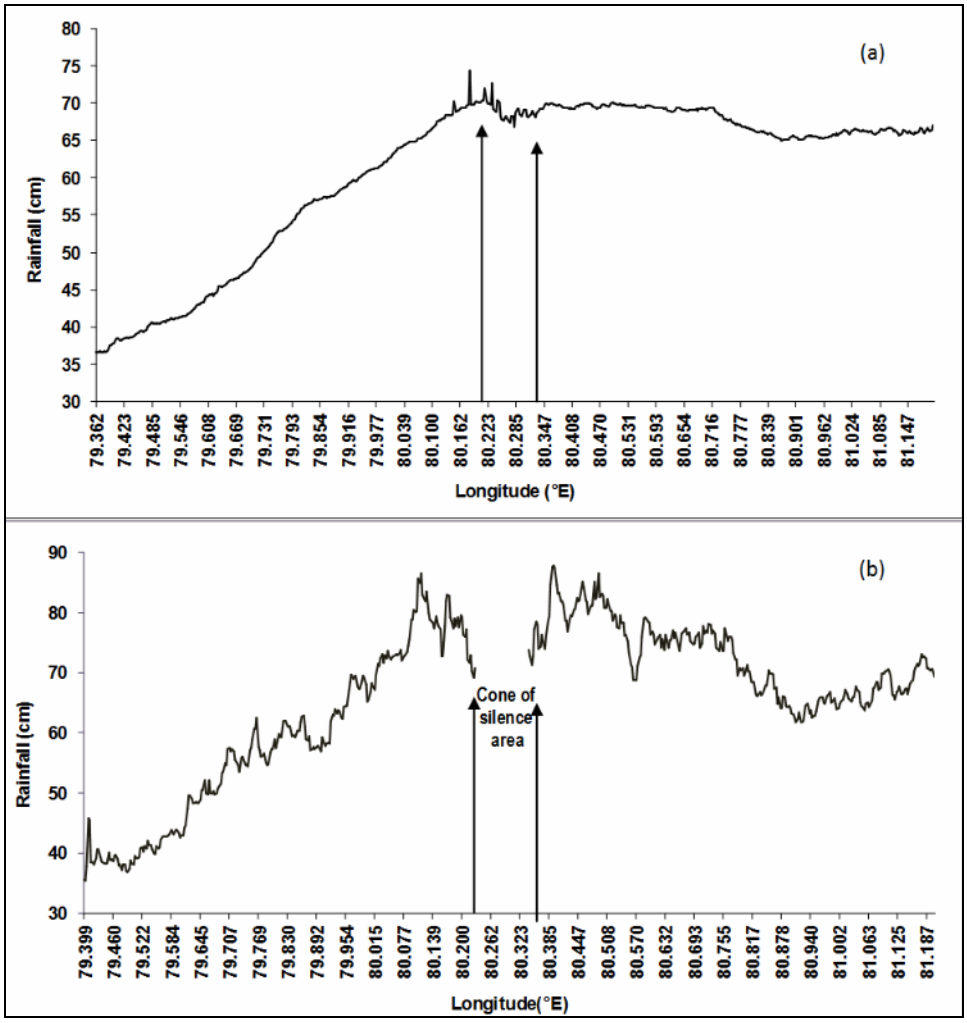

Figs. 10(a&b). Longitudinal variability of mean RERF (cm) over land and ocean during DO-DW of NEM, 2002-13 (a) averaged across all latitudes and (b) at 13.1° N
(The space between the arrows in the above figures indicates areas in and around the coastline)

(*ii*) In the case of Fig. 10(b), the area of the cone of silence is clearly seen and the RERF peaks at nearly 20 km west and east of the coast. The decrease of RERF over the ocean eastwards is sharper than the mean profile depicted in Fig. 10(a) and westwards in the land area also, the decrease in RERF is sharper, linear and similar to Fig. 10(a).

5.4. *Analysis of mean RERF pattern in Dec post-withdrawal of NEM*

During the period 2002-13, NEM withdrew in Dec in 7 out of the 12 years and spilled over to Jan in 5 years (Table 1). The fixing of DW of NEM over CTN has been based on careful analysis of daily RGRF of several stations of south AP and CTN (Raj, 1998a; Geetha & Raj, *loc.cit.*). However, even after the identified DW, some amount of RF might get realised over land itself which may not have been detected by the manual RG network. There has been no authentic study on the quantum of RF received over BoB after the retreat of NEM from land (*i.e.*, CTN). To study the same, using the RERF of 99 post-NEM withdrawal days of Dec, the mean DRERF was computed and the spatial distribution is depicted in Fig. 11.

It is seen that the oceanic areas received more RF compared to land areas. Except for a small patch north of DWR, the land region is almost dry with no substantial contribution of RF to the seasonal NEM. The mean RERF shows increasing RF over BoB as one moves eastwards from the coast. It is well known that NEM prolongs into Jan over the eastern parts of Sri Lanka with stations like Baticaloa (7.7° N / 81.7° E at 3 m a.s.l.) receiving normal

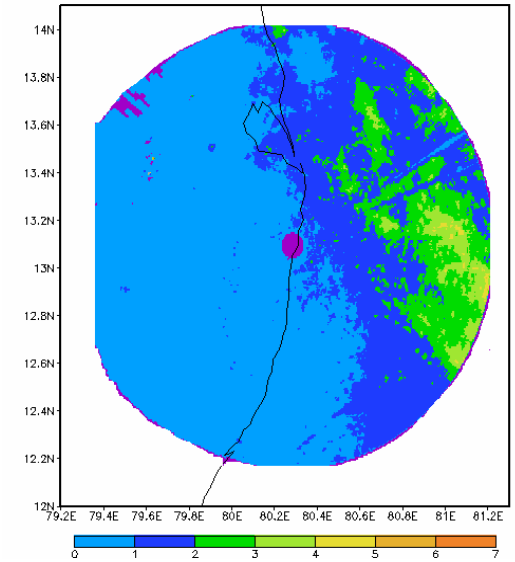

Fig. 11. Mean daily RERF (mm) of post-NEM withdrawal days of Dec, 2002-13

RF of 27 cm. The pattern of NEM withdrawal is by and large from N-S and west to east (W-E). The RERF distribution over BoB as shown in Fig. 11 conforms to the above pattern despite the fact that the data used in the analysis is only up to a distance of 100 km from Chennai DWR.

5.5. *Mean RERF over land and oceanic areas during NEM season, 2002-13*

In the previous sections, the salient features of the spatial distributions of mean RERF for seven different periods were elaborated. Whereas conventional RGRF observations are not available over oceanic areas, RERF observations over BoB are available up to a distance of 100 km from Chennai DWR. Continuing the analysis further, the mean RERF over land and that over ocean based on the grid point values were computed to facilitate ease of comparison. The BoB coast runs almost N-S and so the circular area of 100 km radius was approximately delineated into two semi-circles comprising areas of land and ocean. The RERF values from the 600 × 600 matrix that belong to each semi - circle, numbering nearly 1.43 lakhs, were separately averaged to derive the mean RERF over land and ocean. Such computations were repeated for each of the seven periods and the mean RF values thus derived are presented in Table 4.

As shown, mean RERF over oceanic areas of BoB in the 100 km radius from the Chennai DWR is consistently more than that over land for all the periods. Oct is the rainiest month over the oceanic area with a mean RERF of 357.1 mm when compared to Nov (299.6 mm) and

TABLE 4

Mean RERF over land and ocean during the NEM season of 2002-13

No.	Category	Land	Ocean
		RF (mm)	
1.	Oct	273.3	357.1
2.	Nov	262.2	299.6
3.	Dec	92.5	107.6
4.	NEM season (OND)	628.4	761.4
5.	Pre-NEM days of Oct	66.4	83.0
6.	Duration of NEM (DO-DW)	561.5	680.8
7.	Post-withdrawal days of Dec	0.4	1.9

DO : Date of Onset; DW : Date of Withdrawal

Dec (107.8 mm). However, over land, RERF of Oct (273.3 mm) is almost equal to that of Nov (262.2 mm) while that of Dec is 92.5 mm. During the NEM season (OND) as a whole, oceanic areas (761.4 mm) are rainier than land (628.4 mm). The same pattern is observed during pre-NEM days of Oct with RERF of 83.0 mm and 66.4 mm over ocean and land respectively. During DO-DW, the mean RERF over ocean is 680.8 mm and that over land is 561.5 mm. In the case of post-withdrawal days of NEM, mean RERF over ocean is 1.9 mm while that over land is negligible (0.4 mm). It is seen from Fig. 11 that RERF over the eastern parts of BoB is higher. In all seven cases discussed above, RERF over ocean is higher than that over land. However, there is a deviation from this overall pattern observed, which will be presented in a subsequent section.

5.6. *Mean RF pattern during days of CDs over BoB*

It is well-known from the NEM RF climatology that CDs which form and move over BoB are major synoptic systems associated with active NEM conditions over TN and adjoining areas. Apart from these migratory systems, active NEM is also associated with strong low level easterly winds. When CDs are present over the ocean, that substantial RF should occur over the oceanic areas affected by the CDs is obvious. As RERF is available over the area of concern in BoB, it is of interest to study the RERF pattern over the ocean *vis-à-vis* land when NEM is active over the land with or without CDs present over BoB. The spatial distribution of RERF discussed in Section 5.3.2 for DO-DW of NEM includes CD days also. During Oct-Dec (2002-2013), as many as 36 systems formed or moved over BoB. In the case of the duration of NEM, 26 days associated with 17 CDs which originated/ moved/crossed in the 400 km distance from Chennai DWR, as listed in Table 2 have been identified as

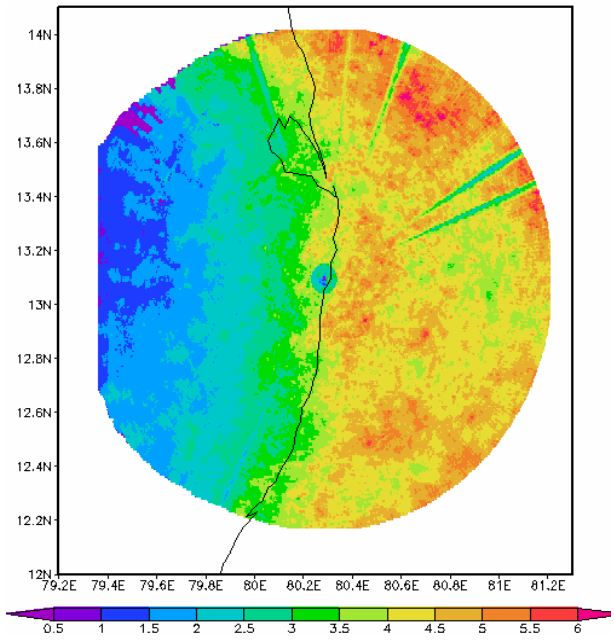

Fig. 12. Mean daily RERF (cm) within 100 km of Chennai DWR, under the influence of CDs of BoB during DO to DW of NEM, 2002-13

causing normal or higher level of NEM RF activity over land. The tracks of the 17 CDs are displayed in Figs. 3(a&b). The spatial distribution of mean DRERF averaged over the 26 CD days in BoB during DO-DW for each grid point was generated and is presented in Fig. 12. Mean DRERF > 4 cm on CD days is observed over large parts of the ocean. Land areas close to the coast have DRERF of the order of 3.0-3.5 cm while few patches of RF 4-4.5 cm just a few km away from the coastline are observed. The mean DRERF values computed for the semi-circular areas of both the ocean and land are 4.4 cm and 2.2 cm respectively indicating that during CD days, oceanic areas of BoB over the region of study receive approximately two times more RF than land areas. A rapid decrease in RF over land from coast to inland is evident from Fig. 10. Further, it is inferred from Figs. 9&12 that when RF due to CDs is excluded, the RERF realised during DO-DW is lesser approximately by 2 cm over land and by 4 cm over ocean.

5.7. *Spatial variation of RERF during various phases of NEM*

The NEM season is generally interspersed with 4-5 active spells of RF with dry spells in between. Some of the dry spells could last for a prolonged duration. The seasonal RF realised is largely dependent upon the number of active spells of RF. When high resolution data is available from DWR, it is possible to analyse the RF

TABLE 5(a)

Description of spatial distribution of DRF over a region

Classification	Percentage of number of rain gauge stations reporting DRF of at least 2.5 mm
Dry (D)	Nil
Isolated (I)	≤ 25%
Scattered (SC)	26-50%
Fairly Widespread (FW)	51-75%
Widespread (W)	≥76%

TABLE 5(b)

Description of strength of the monsoon over a region for a day

Category	Ratio of DRF realised with reference to normal DRF
Dry	No rain
Weak	≤ 0.5
Normal	0.5 -1.5, SC
Active	>1.5-4, FW / W
Vigorous	>4, FW / W

Note : Definitions given in Tables 5(a&b) are as per IMD, DRF : 24 hrs daily rainfall

estimates over the region of study to understand the mesoscale variations in RF during the various phases of NEM activity. In order to determine the strength and spatial distribution of NEM within the 100 km radius of the DWR, the DRF recorded by 34 RG stations have been used (Fig. 2).

During the period 2002-13, TN had a continuous run of positive RF PDNs during 2004-11 with several excess years (PDN + 20% or more) as shown in Table 1. IMD describes the spatial DRF distribution over a region as dry, isolated, scattered, fairly widespread and widespread (for a day, based on 24 hrs CRF ending at 0830 hrs IST). The strength of NEM is termed as Dry, Weak, Normal, Active or Vigorous as per IMD nomenclature and classifications which are defined in Tables 5(a&b). Using the long term (1951-2000) normals of DRF (NDRF) of 20 stations (IMD, 2010), the NDRF values for the remaining 14 stations were interpolated.

The NDRF for the NEM season 1 Oct- 31 Dec computed for the region within the 100 km radius of the Chennai DWR as a mean of RGRF data of 34 stations in the area is presented in Fig. 13. The mean RGRF of a day was computed based on the number of stations for which RF data was available. The ratio of actual RF to NDRF was calculated for each day. The strength and spatial

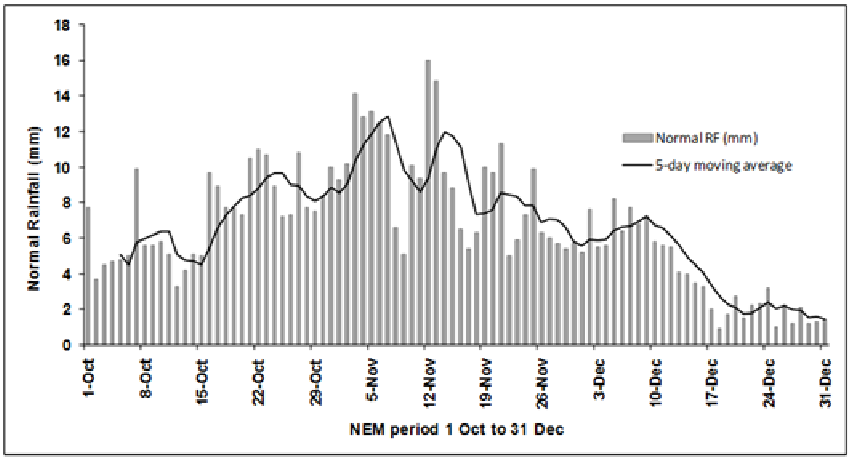

Fig. 13. Normal daily RGRF (mm) over land within 100 km of Chennai DWR based on data of 34 stations, for 1 Oct - 31 Dec

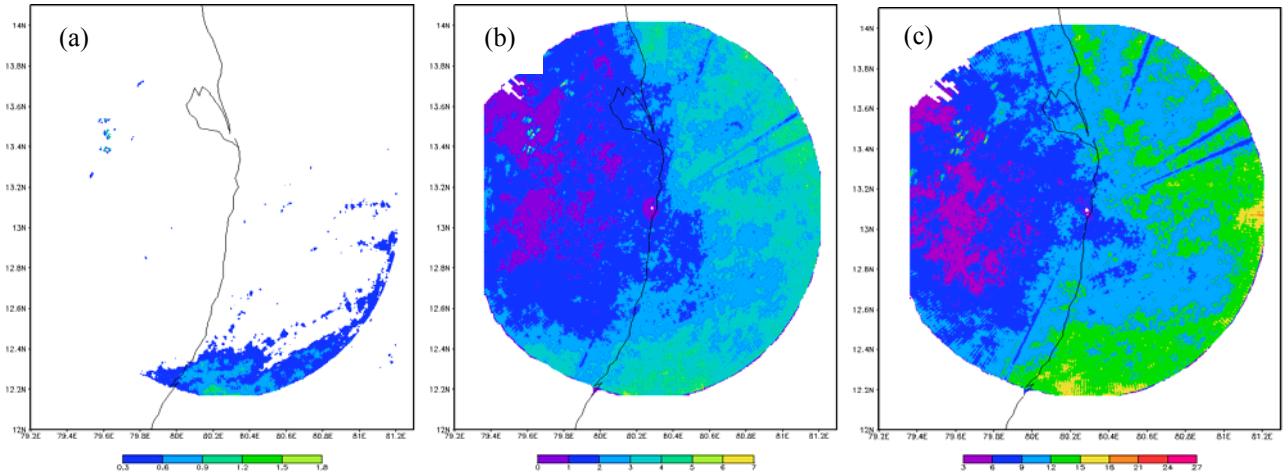

Figs. 14(a-c). Mean daily RERF (mm) associated with (a) dry (b) weak and (c) normal NEM activity during 2002-13

distribution of NEM were determined for each day and year to identify the days of various types of NEM activity. During the 12 year period 2002-13 of the NEM season, data was available for 1079 out of 1104 days save for 25 days of missing data. The numbers of days of dry, weak, normal, active and vigorous phases of NEM are 309, 399, 206, 99 and 66 respectively (Table 6). The daily RERF values of the days falling under dry, weak and normal NEM activity were averaged to generate the categorywise spatial mean RERF patterns that are depicted in Figs. 14(a-c). The features are described below:

Dry : In the case of dry days [Fig. 14(a)] almost the entire area in the 100 km range of the DWR is rain-free except for a patch of mean DRERF < 1 mm in the southern sector over the ocean, close to the coast.

Weak : During weak NEM days [Fig. 14(b)], mean DRERF up to 2 mm near the coast decreases to 1 mm westwards. The oceanic areas have DRERF of 2-7 mm.

Normal : In the case of normal NEM days [Fig. 14(c)], an increase in DRERF in the range 9-12 mm along the entire coast of BoB is observed. A gradual decrease in DRERF from coast to inland up to 3 mm is discernible over land, whereas over ocean the RF activity is spatially widespread with southern and easternmost patches indicating DRERF up to 18 mm.

Active : During active NEM days [Fig. 15(a)], an almost uniform distribution of DRERF in the range 1.5-2 cm over both land and ocean is observed except for significant patches of 2-2.5 cm in the SW (over land) and

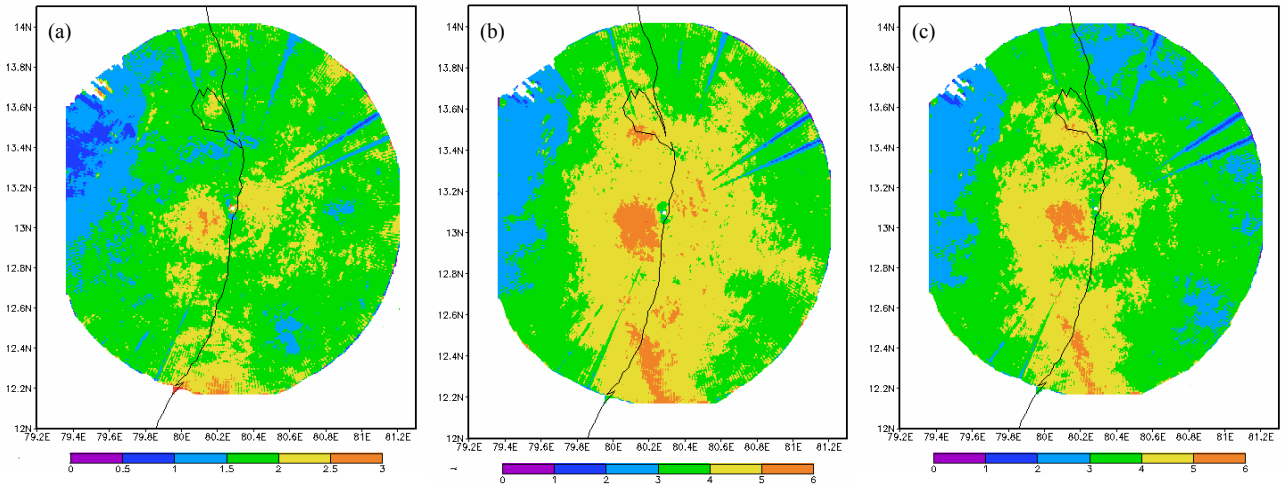

Figs. 15(a-c). Mean daily RERF (cm) associated with (a) active (b) vigorous NEM activity (c) both active and vigorous days combined excluding 14 CD days

TABLE 6

Number of days of DWR data availability for the various phases of NEM activity during 2002-13

Month	Northeast monsoon activity, 2002-13					Total data used
	Dry	Weak	Normal	Active	Vigorous	
Oct	33	162	100	51	19	365
Nov	93	147	59	37	23	359
Dec	183	90	47	11	24	355
Total	309	399	206	99	66	1079
Missing data : 25 days						
Total : 1079 + 25 = 1104 days						

NE (over ocean) sectors between 79.8 - 80.6° E and 12.8-13.2° N. The southern sector also has a zone of DRERF of 2-2.5 cm with a small patch of 2.5-3 cm along the periphery of the DWR range. The SW sector a few km inland from the coast also has a distinct high RF patch of 2.5-3 cm.

Vigorous : In the case of vigorous days of NEM [Fig. 15(b)], a spatially uniform mean DRERF of 4-5 cm is realised over larger areas of both land and ocean. Distinct patches of higher RF of 5-6 cm are observed both over land in the SW sector of the DWR location and over ocean in the SSE sector. Decrease in DRERF up to 2 cm further westwards inland is noticed.

It is well-established that presence of CDs in BoB for 2-3 days increases the RF over the coastal areas drastically and so identifying the influence of CDs on the RF activity during NEM season becomes important. Hence, the analysis was further continued by excluding 14 CD days (out of which 8 are in active and 6 in vigorous phase) from the active (99) and vigorous (66) NEM days and averaging 151 [(99 + 66) – (8 + 6)] days of DRERF for which data was available, to generate a mean RERF distribution as given in Fig. 15(c).

After removal of RF due to CD days, it is observed that DRERF due to active and vigorous (AV) NEM days is conspicuously higher (4-5 cm) over or close to the coast and adjoining land areas than that over ocean. RERF of 4-5 cm extends up to 30 km west of the coast inland but decreases sharply further westwards. Over the ocean, the DRERF of 4-5 cm extends up to only around 15 km eastwards that too predominantly in southern latitudes. In northern latitudes, DRF is 3-4 cm only even over the ocean but further decrease is gradual. Clearly and expectedly, removal of RF due to CD days has reduced the RF over ocean.

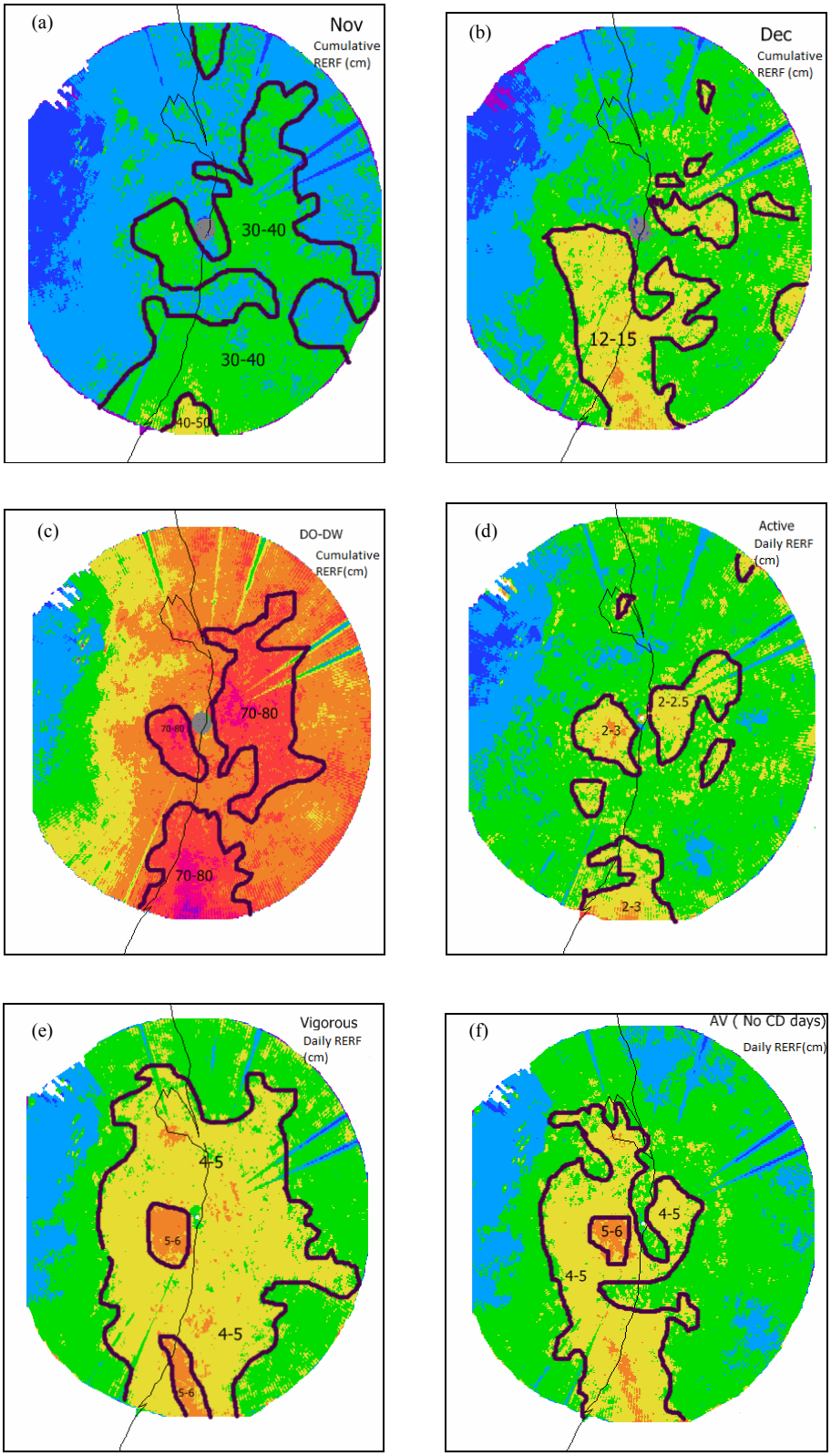

Figs. 16(a-f). Mosaic of cumulated mean RERF (cm) of (a) Nov, (b) Dec, (c) the period between DO to DW and daily mean RERF (cm) associated with (d) active (e) vigorous and (f) active and vigorous NEM days excluding CD days

Some of the other salient results of this analysis are:

(*i*) The mode in DRERF occurs 5-10 km SW of Chennai DWR near BoB coast with the presence of a very high RF patch of 5-6 cm which is clear from both Figs. 15(b&c). The patch of higher RF is not exactly over the coast during AV NEM days.

(*ii*) During AV NEM days without CDs, land areas have received comparatively more RF than ocean.

In all the phases *viz*., normal, active, vigorous and AV minus CD days of NEM activity, isodop effect (Section 4.3.2) of varying dimensions and scales and underestimation of RERF due to obstructions manifested as conical beams as explained in Section 4.3.1 have been observed.

The high RERF pattern in the SW sector of the DWR is seen in Fig. 9 (DO-DW) as well but the extent to which such a signature would be present if the zero isodop effect were nullified is a bit obscure. However, for vigorous and AV NEM days [Figs. 15(b&c)], the pattern is clearly defined and would be so despite the isodop effect. If such a feature of higher RERF observed in the SW sector of the DWR location is not an artifact of DWR system, a plausible physical reasoning could be that the SW sector of Chennai city is highly urbanised with a large number of high rise buildings compared to north or NW sectors. The resulting contribution of higher roughness parameter to increased frictional convergence and hence slightly higher RF appears as a reasonable explanation.

5.8. *Region of heaviest NEM RF over BoB - Comparison with satellite data based findings*

It is well-known from NEM climatology that RF during NEM is higher over coast and decreases inland. This feature which can be appraised from the normal RF pattern is also frequently observed during active NEM conditions [IMD (1973) & Raj (2012)]. In this study based on RERF, it has been possible to bring out the sharp decrease of RF inland [Fig. 7(a)]. It is of tremendous interest and scientific curiosity to get an insight on the quantum of RF realised over the oceanic areas adjacent to CTN during the NEM and its various phases. In the absence of RGRF data over oceans, remote sensing methods which provide RF directly or through some proxy parameter are the other options available. Suresh and Raj (2001) based on three years (1996-98) of OLR data of resolution 80 km × 80 km obtained from NOAA polar orbiting satellites showed that the RF profile during active NEM conditions displayed a maximum over CTN, decreasing sharply inland and gradually eastwards over ocean. Amudha *et al.* (2016b) using 13 years (2000-12) of INSAT OLR data of 1°×1° resolution conducted a detailed analysis and reiterated the same result. In both the studies OLR was taken as a proxy for RF.

It is important to examine whether the above feature of NEM RF as derived from OLR observations emerges when analysis is based on RERF data of very high resolution, *i.e*., 333m × 333 m. The mean RERF distributions presented in Figs. 6(b&c), 7(a), 9, 10(a), 15(a-c) were critically evaluated to detect such a pattern, if any. A mosaic of the above figures (excluding Figs. 7(a) and Fig. 10(a) clearly demarcating through isohyets, the higher RERF regions is presented in Fig. 16. For colour coding and finer details, original figures may be referred.

The inferences drawn from the above figures are described below:

It is seen from the RERF distribution for Nov and Dec that over the ocean, the heaviest RERF values are observed within 40 km from the coast with some decrease further eastwards. Almost similar pattern is seen in the normal RERF distribution for the NEM (OND) season. Figures depicting the normal RERF distribution for DO-DW and Fig. 10(a) which displays the mean longitudinal distribution also clearly illustrate this feature. In Fig. 10(a), the highest RF during DO-DW of NEM occurs in the stretch which extends nearly 30 km west of the coast into the land (65-72 cm) and 40 km east of the coast into the ocean (67-68 cm) beyond which RF decreases (62-65 cm). Overall, the quantum of RERF decrease in the ocean in the eastern region compared to coastal regions is only around 8% but the pattern is well-defined and clearly marked. Further reiteration is clear from Figs. 15(a-c) depicting the spatial distribution of mean DRERF on active, vigorous and AV days excluding RERF due to CDs.

In view of the high resolution of the data used and the well-known property that RF varies considerably in space and can have discontinuities even if averaged, sometimes the spatial distributions which are presented do not give a smooth profile and there might be patches of RF which deviate from the conceptual pattern described as above. However, the overall feature that RF is heaviest over CTN and neighbourhood stands reiterated. Yet another authentic evidence of the above characteristic is provided by the comparison of the mean RERF during DO-DW (Table 4) over the semi-circular region of the ocean and the mean coastal RERF computed from the data of several representative points along the coast (Fig. 9). The former is 68 cm and the latter 75 cm. These figures clearly indicate that the quantum of RF realised over eastern parts of the semi-circular oceanic region is lower when compared to that along the coast.

The two studies by Suresh & Raj (2001) and Amudha *et al.* (2016b) based on OLR data could not precisely delineate the extent of high RF closer to CTN based they are of lower resolution satellite data when compared to the resolution of RERF (333 m × 333 m). With higher resolution RERF data, it has become possible to delineate the high RF zone which approximately extends 25-30 km west of the coast into land and around 30-40 km east of the coast over the ocean as deduced from the various figures and elaborations in the previous sections. It must be stated that the analysis based on OLR data covered almost the entire BoB and extended up to southern latitudes whereas reliable RERF data is available only up to 100 km from the Chennai DWR location and for lesser distances in other latitudes of the area of consideration. Notwithstanding such a limitation, both the reiteration of the OLR based features and the delineation of high RF zone based on RERF analysis are interesting results emerging from this study.

6. Remarks

While analysing the RF characteristics of NEM extracted from RERF and arriving at conclusions as elaborately discussed above, various aspects of DWR instrumental configurations and calibration procedures have been taken into account. Huge volume of data has been processed by carefully eliminating noise in the data though few artifacts as mentioned in Section 4.3 could not be eliminated totally. Despite the advantage of using Doppler clutter filters during the sampling which outweighs its disadvantages, high intensity echoes do creep in which cannot be totally avoided as observed from the data used in the analysis.

RF is spatially and temporally a highly variable parameter. Climatologically, 30-50 years of continuous data is needed to derive normals representative of the behaviour of a meteorological parameter over the specific location of study. The present analysis pertaining to the 12 year period, 2002-13 is too short a period to derive inferences which can be taken as general features. In addition, this period had a historically high positive epoch of RF years 2004-11 for TN and for the region of consideration which possibly could have induced some amount of bias in the results derived. Despite such limitations, it is remarkable that seemingly consistent results have emerged from this study.

A DWR typically generates data on several other parameters also aside from RF. The DWR network maintained by IMD is quite expansive, generating huge amount of data every day. The present study is a first of its kind undertaken in India to study climatological features of NEM and to derive a few new results by utilising DWR products generated over more than a decade. Needless to say that there is tremendous scope to pursue more research based on the voluminous and wide spectrum of DWR data.

7. Summary

The results of the study are summarised as under:

(*i*) The DWR at Chennai operational with effect from Feb 2002 is located on the BoB coast and provides reliable RERF for a circular area of nearly 100 km radius covering both land and oceanic areas on either side of the DWR location. Among the several radar products generated by the DWR, the major database used for this study is the 12 years (2002-13) daily PAC product for the NEM period of 1 Oct to 31 Dec. The resolution of the data used is 333 m × 333 m. PAC provides a spatial distribution of cumulative RERF for 24 hours duration ending at 0830 hrs IST. Over 2.8 lakhs of grid point data per day has been processed. RF data of 34 land based RG stations is used for comparison between RERF and RGRF and for identifying the various phases of NEM activity.

(*ii*) Spatial distributions of mean RERF were generated for Oct, Nov and Dec. In Oct, over land, RERF is 20-30 cm while NW sector has patches of lower RF of 10-20 cm. Areas closer and along the coast, receive RF of 30-40 cm while NE sector over ocean has RF of 40-50 cm. In Nov, land areas south of the DWR receive RF of 30-40 cm compared to north while more of oceanic areas receive the same amount of RF. In Dec, there is a conspicuous gradual decrease in RERF over land from 12-15 cm close to the coast in the southern sector to 3-6 cm westwards, in the NW sector. In most of the oceanic area, RERF is greater than 9 cm.

(*iii*) Spatial distribution of seasonal OND mean RERF is heavier in the range 80-90 cm closer to the coast. Heaviest RF patch of 90-100 cm is observed in the SW sector few km inland. From the DWR location, RERF decreases E-W and southern latitudes receive 10-15% more RF than the northern latitudes. Over the ocean, heaviest patches are in the NE sector. Decrease of RF eastwards is gradual. The 12 years (2002-13) mean OND RERF over the ocean is 761 mm which is 18% higher (by 133 mm) than that over land which is 627 mm. Climatologically, the OND seasonal RF is generally heavier over the coast and decreases westwards inland and this feature has been realised in the seasonal mean OND RERF distribution very well.

(*iv*) The RERF retrieved from the grid points of the 34 stations and averaged is 629.8 mm whereas the OND mean RGRF computed for the 34 stations is 627.4 mm

yielding a difference of just 2.4 mm or 0.4% of mean RGRF. The MAD is 69.2 mm which is 11% of the mean RGRF. The CC between RERF (x) and RGRF (y) is 0.82 which is highly significant.

(*v*) In the pre-NEM days of Oct, average RERF over land and ocean are 4-8 cm and 8-12 cm respectively. The RF during pre-NEM days contributes to 10% of the seasonal total OND RF. The normal pattern of relatively higher RF over CTN during NEM is not observed in the pre-NEM RERF distribution.

(*vi*) The RERF for the duration of NEM (DO-DW) is 10-20 cm less than that of the mean RERF for the OND seasonal mean. For given latitude, the RERF is higher close to the coast and decreases westwards almost linearly, with a maximum RF of 80-90 cm in a patch in the SW of the DWR location.

(*vii*) During DO-DW, the mean RERF is 68 cm in the semi-circular region of the oceanic areas and is 75 cm for stations located on the coast. The region just close to the coast receives 10% more RF than oceanic area.

(*viii*) Mean RERF of post-withdrawal days of Dec has indicated more RF in eastern BoB which increases as one moves eastwards from the coast. This RERF distribution is consistent with the normal pattern of withdrawal of NEM over BoB from N-S and W-E.

(*ix*) The spatial distributions of mean RERF over land and ocean analysed for the several categories clearly indicate that RERF over ocean is higher than that over land. However, during DO-DW, the RERF in the coastal areas is heavier than that over ocean.

(*x*) During CD days, DRERF > 4 cm is observed over oceanic areas, with a rapid and sharp decrease of up to 1 cm over land westwards from the coast. Oceanic areas receive a mean DRERF of 4.4 cm which is twice that over inland areas (2.2 cm).

(*xi*) During dry phase of NEM, land area in the 100 km range of the DWR is almost devoid of RF. During weak NEM days, mean DRERF is up to 2 mm near the coast which further decreases to 1mm westwards. In the case of normal NEM days, an increase in DRERF in the range 9-12 mm along the entire coast of BoB is observed.

(*xii*) During active NEM days, an almost spatially uniform RF distribution with a small area of DRERF 2.5-3 cm inland and SW of the radar location is discernible. Vigorous NEM days receive DRERF of 4-5 cm in large areas over land and ocean close to the coast with significant patches of high RF up to 6 cm in the SW/S sectors.

(*xiii*) In the case of AV NEM days excluding the CD days, the substantial reduction in RF over the oceanic region in contrast to the spatial distribution of RF of vigorous days of NEM has been perceptibly brought out. Area covered by RERF of 4-5 cm is more inland close to the coast than ocean.

(*xiv*) The presence of a relatively high DRERF patch of 5-6 cm approximately 5-10 km west of the coast inland in the SW sector of Chennai DWR is identified during both vigorous and AV NEM days excluding RF due to CD days. This feature could possibly be attributed to increase in roughness parameter aided by substantial urban development over the area of Chennai city leading to frictional convergence and hence higher RF.

(*xv*) It has been conclusively shown in this study, using a different type of approach that during DO-DW and also during active and vigorous spells, the zone of heaviest RF is almost along the N-S belt extending 25-30 km west of the coast over land and 30-40 km east of the coast over ocean. East of this stretch, RF shows a small but clearly defined decrease over the ocean. This result reiterates and compares favourably with similar conclusions drawn in two earlier studies of NEM based on satellite OLR data.

Acknowledgement

The authors thank the Dy. Director General of Meteorology, RMC Chennai for having provided the facilities for the study. The first author is grateful to the officers and staff of DWR, Chennai for their wholehearted support and indebted in particular to Shri V. Aravindan for his commitment in processing and generating the text files of PAC from the raw data. The authors thank Shri RM. A. N. Ramanathan, Asst. Meteorologist, RMC Chennai for his guidance in generating GrADS imageries and Shri M. Bharathiar, S.A. for drawing some of the figures depicted in the study.

References

Amudha, B., Raj, Y. E. A., Thampi, S. B. and Ramanathan, RM. A. N., 2014, "A diagnostic and statistical approach to the validation of Doppler radar RF around Chennai during 2006-10", *Indian Journal of Radio and Space Physics*, **43**, 163-177.

Amudha, B., Raj, Y. E. A. and Asokan, R., 2016a, "Characteristics of movement of low level clouds associated with onset / wet spells of northeast monsoon of Indian sub-continent as derived from high resolution INSAT OLR data", *Mausam*, **67**, 2, 357-376.

Amudha, B., Raj, Y. E. A. and Asokan, R., 2016b, "Spatial variation of clouding / rainfall over southeast Indian peninsula and adjoining Bay of Bengal associated with active and dry spells of northeast monsoon as derived from INSAT OLR data", *Mausam,* **67**, 3, 559-570.

Bhatnagar, A. K., Rajesh Rao, P., Kalyanasundaram, S., Thampi, S. B., Suresh, R. and Gupta, J. P., 2003, "Doppler Weather Radar - A detecting tool and measuring instrument in meteorology", *Curr. Sci. (India)*, **85**, 256-264.

De, A. C. and Rakshit, D. K., 1961, "Radar observations on the formation of cumulus clouds near Calcutta during monsoon season', *Indian J. Met. Geophys.,* **12**, 289-298.

Geetha, B., 2011, "Ph.D thesis, Indian northeast monsoon as a component of Asian winter monsoon and its relationship with large scale global and regional circulation features", University of Madras, Chennai.

Geetha, B. and Raj, Y. E. A., 2015, "A 140 year data archive of dates of onset and withdrawal of northeast monsoon over coastal Tamil Nadu", *Mausam*, **66**, 1, 7-18.

India Meteorological Department, 1973, "Northeast monsoon", FMU Report No. IV-18.4.

India Meteorological Department, 2010, Daily rainfall normals, 1951-2000, CD format, Pune.

India Meteorological Department, 2011, "Cyclone e-Atlas", Version 2, Tracks of cyclones and depressions over north Indian Ocean, Chennai.

Kulshrestha, S. M. and Jain, P. S., 1967, "Radar climatology of Delhi and neighbourhood - occurrence of severe weather", *Indian J. Met. Geophys.,* **18**, 105-110.

Lakshmanaswamy, B. and Sundaresa Rao, V., 1974, "Radar climatology of Madras airport and its neighbourhood", *Indian J. Met. Geophys.,* **25**, 461-467.

Marshall, J. S. and Palmer, W. McK., 1948, "The distribution of raindrops with size", *J. Meteor. (USA)*, **5**, 165-166.

Mukerjee, A. K., Kumar, S. and Krishnamurthy, G., 1977, "A radar study of growth and decay of thunderstorms around Bombay during the pre-monsoon season, "*Indian J. Meteor. Hydrol. Geophys.,* **28**, 475-478.

Nan, L. B. and Ming, W., 2010, "An automated velocity dealiasing method based on searching for zero isodops", *Q. J. R. Meteorol.Soc.*, 3, Part B, **136**, 1572-1582

Pankajkumar, 2006, "Northeast monsoon rainfall prediction", Ph.D Thesis, Pune University.

Probert-Jones, J. R., 1962, "The radar equation in meteorology", *Q.J.R. Meteorol. Soc*., **88**, 485-495. doi: 10.1002/qj.49708837810.

Raghavan, S. and Varadarajan, V. M., 1981, "Radar estimate of rainfall and latent heat release in tropical cyclones of Bay of Bengal", *Mausam*, **32**, 3, 247-252.

Raghavan, S. and Sivaramakrishnan, T. R., 1982, "Radar estimation of precipitation around Madras, *Mausam*, **33**, 1, 21-28.

Raghavan, S., Sivaramakrishnan, T. R., Rengarajan, S. and Kumar, S. W. P., 1987, "A radar reflectivity-rainfall rate relationship for the southwest monsoon season for the Madras area", *Mausam*, **38**, 3, 335-340.

Raghavan, S., 2003, "Radar Meteorology", ISBN 1-4020-1604-2, (Kluwer Academic Publishers, Netherlands), 262-264.

Raj, Y. E. A., 1992, "Objective determination of northeast monsoon onset dates over coastal Tamil Nadu for the period 1901-90", *Mausam*, **43**, 3, 272-282.

Raj, Y. E. A., 1998a, "A scheme for advance prediction of northeast monsoon rainfall of Tamil Nadu", *Mausam,* **49**, 2, 247-254.

Raj, Y. E. A., 1998b, "A statistical technique for determination of withdrawal of northeast monsoon over coastal Tamil Nadu", *Mausam,* **49**, 3, 309-320.

Raj, Y. E. A., 2003, "Onset, withdrawal and intraseasonal variation of northeast monsoon over coastal Tamil Nadu, 1901-2000", *Mausam*, **54**, 3, 605-614.

Raj, Y. E. A., Asokan, R. and Revikumar, P. V., 2007, "Contrasting movement of wind based equatorial trough and equatorial cloud zone over Indian southern peninsula and adjoining Bay of Bengal during the onset phase of northeast monsoon", *Mausam*, **58**, 1, 33-48.

Raj, Y. E. A., 2012, Monsoon Monograph, Vol.I, India Meteorological Department, Pune, Ch.13.

Rajesh Rao, P., Kalyanasundaram, S., Thampi, S. B., Suresh, R. and Gupta, J. P., 2004, "An overview of first Doppler Weather Radar inducted in the cyclone detection network of India Meteorological Department", *Mausam*, **55**, 155-176.

Rinehart, R. E., 1991, "Radar for Meteorologists", Part III, 2nd ed., University of North Dakota, USA.

Suresh, R., Ravichandran, P. K., Gupta, J. P., Thampi, S. B., Kalyanasundaram, S. and Rajesh Rao, P., 2005, "On optimum rain rate estimation from a pulsed Doppler Weather Radar at Chennai", *Mausam,* **56**, 433-446.

Suresh, R. and Raj, Y. E. A., 2001, "Some aspects of Indian northeast monsoon as derived from TOVS data", *Mausam*, **52**, 4, 727-732.